THESIS

SINGLE POWER SUPPLY OPERATION OF A HALL THRUSTER

Submitted By:

Zachary K. Robertson

Department of Mechanical Engineering

In partial fulfillment of the requirements

For the Degree of Master of Science

Colorado State University

Fort Collins, Colorado

Fall 2024

Master's Committee:

Advisor: John Williams

Doug Fankell
Jacob Roberts

ABSTRACT

SINGLE POWER SUPPLY OPERATION OF A HALL THRUSTER

Interest in operating Hall thrusters with a single power supply, facilitated by heaterless hollow cathodes, has motivated this research. Initial investigations into the Safran PPS 1350 confirmed the potential for this configuration. Building on these findings, modifications were made to a laboratory Hall thruster to enable operation with a single power supply and changes were made to the electrical configuration to promote smooth cathode ignition and decrease the influence of the inductance in the magnetic coils. In addition to operating with a laboratory power supply, CisLunar Industries supplied a prototype anode supply that demonstrated capability of running the laboratory Hall thruster under these conditions without efficiency losses, as verified by thrust stand data. A phenomenological efficiency analysis was performed using a Faraday probe and a retarding potential analyzer which supported these results, while also providing pertinent sub-efficiencies. The study concludes that a single power supply configuration is a viable approach to starting and operating a Hall thruster equipped with a heaterless hollow cathode.

TABLE OF CONTENTS

CHAPTER 1: INTRODUCTION

Hall thrusters offer significant propellant savings for ambitious space missions due to their high specific impulse, however their operation requires multiple power supplies be used to provide independent control of the cathode-anode discharge, cathode-keeper discharge, magnetic coils, cathode temperature, and gas flow. Previous work has been done to allow the magnetic coils and gas flow control to be wired in series with the anode discharge to eliminate the need for these separate power supplies. More recently, work done at Colorado State University has shown that hollow cathodes can be started instantly without using a heater to preheat the cathode [1]. These techniques, when combined, would allow operation of a Hall thruster with a single power supply consisting of a single positive and negative lead, which was first documented in a patent issued to Martinez et al [2]. The benefits of this are a lighter and simpler power processing unit for flight, which would decrease cost and reduce the propulsion system mass.

A Safran PPS 1350 was configured to be operated as described by claim 15 of the Martinez et al. patent and tested in the Orion Vacuum Test Facility at the Center for Electric Propulsion and Plasma Engineering (CEPPE) at Colorado State University. This configuration was demonstrated to start and operate with the use of a single power supply provided by CisLunar Industries and an instant start hollow cathode provided by Plasma Controls, who has licensed the cathode technology from CSU. The demonstration of this capability has inspired continued interest from Safran and CisLunar, and work continued in the CEPPE lab to modify a kW-class, laboratory-model Hall thruster to operate in the single power supply configuration. Accordingly, the purpose of this thesis was to investigate and report on the performance of the lab thruster while being operated with a single power supply and with multiple power supplies.

This work presents the thrust-stand measured anode efficiencies and plasma-diagnostic-derived phenomenological efficiencies of the thruster at a single operating condition and compares the use of a single power supply to the operation with individual power supplies controlling the magnet coils, keeper, and anode discharge. The solenoid operated gas valve and flow control system was not included as part of this study, as this has been done by others and does not affect the performance of the thruster. The measured anode efficiency of the thruster was calculated from the thrust measured by a double pendulum nulling thrust stand, mass flow measurements from a flow controller, and measurements of the discharge current and anode voltage. Far field plume measurements were made using a magnetically shielded Faraday probe and a retarding potential analyzer, which were mounted to separate, in-vacuum motion stages. In conjunction with the measurements of force, flowrate, and power to calculate thruster efficiency; the individual phenomenological efficiencies comprising the total thruster efficiency were derived from probe measurements following Huang et al to inform the effects of single power supply operation.

CHAPTER 2: PREAMBLE AND MOTIVATION

The following paragraphs summarize our early, single-power-supply operation of a Safran PPS 1350 thruster where we identified areas of concern about this technique. This early work informed the testing of our laboratory-model thruster and the modifications we made to it, and information is being provided here as a precursor to the discussion of our improved methods.

Preliminary Work with the Safran PPS 1350

The Safran PPS®1350 is a 1.5-kW-class Hall thruster. It was first flown on board ESA's Smart-1 lunar mission in 2003 [3] and remains to date in production for commercial space missions. The magnetic design features electromagnet coil current that is equal to the discharge current over the standard operating regimes, so that the inner and outer coils can be wired in series with the discharge circuit.

A sketch of the single power supply electrical configuration used to test the PPS 1350 is shown in Figure 1. The positive lead of the power supply was connected to a $0.1\ \Omega$ resistor that was placed in series with a $62\ \mu H$ inductor. A $100\ \Omega$ resistor was placed in parallel with the inductor to moderate its current blocking effects. The inductor was then connected to the anode lead and to one side of a $10\ \mu F$ capacitor. The magnet coils of the thruster were wired in series and were connected between the negative output of the power supply and the other side of the $10\ \mu F$ capacitor, which was also connected to the cathode. This connection scheme placed the thruster coils on the power supply side of the RLC filter. The positive terminal of the capacitor, which was tied to the thruster anode, was also connected to the keeper with a $200\ k\Omega$ resistor. A 4-channel oscilloscope was used to record the discharge voltage and discharge current on the

thruster side of the filter, and the magnet coil voltage and current during startup and during steady state operation.

The power supply was switched on and a momentarily high flow rate of propellant was flowed through the instant start hollow cathode to initiate a plasma discharge. The open circuit voltage of the CisLunar power supply was 540 V, and, right before any current began to flow from the cathode to the keeper, the full output voltage was applied to the keeper. This was sufficient to ignite the cathode, and, with propellant also flowing through the thruster anode, start the thruster. The anode voltage was immediately reduced to the desired operating voltage of 300 V, however, due to the relatively rapid increase in current through the circuit and the relatively large inductance of the magnet coils, a relatively large back-EMF was created across the coils. This is of concern because large voltage differences between the coils and the thruster body may cause the coil insulation to break down. This also pushes the cathode to a positive potential for a moment at startup, and this may cause it to interact electrically with the thruster body or the vacuum chamber in an erratic manner.

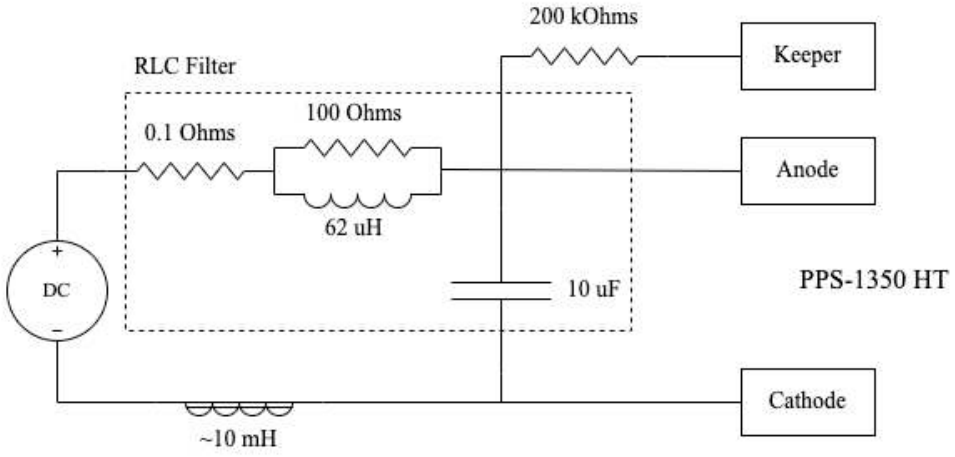

Figure 1. Single power supply configuration used to test the PPS 1350 Hall Thruster.

During steady state thruster operation, it was also determined that the filter did not completely smooth the current flowing through the power supply and coils. Specifically, a ~1 A

peak-to-peak oscillation was observed on the ~5 A average current passing through the coils. This 20% oscillation would change the magnetic field in the channel and may have an influence on the performance of the thruster, as well as consuming more power due to the impedance in the coils and AC-core losses in the bobbins. Although, at such low frequencies, it is expected that the AC-core loss is negligible.

The PPS 1350 was operated in the single supply configuration on Xenon at 1,350 and 1,500 watts. From initial analysis of the data, it appeared that the performance was slightly less than what was recorded while operating with multiple supplies, however, the uncertainty of the thrust measurement due to systematic error was high enough to make up for the difference observed. Since these tests, work has been done to improve the uncertainty of the thrust measurements, which is now ~1 mN at the nominal thrust point of the laboratory model thruster.

Modifications to the Laboratory Thruster and Single-Power Supply Circuit

The laboratory Hall thruster was modified to improve its performance and stability. First, additional wraps were added to the center coil to balance the magnetic field and reduce the current needed to produce sufficient fields, enabling the coils to be run in series with the discharge. Polyimide insulated wire, rated for use up to 400^{o} C, was used for both the inner and outer coils. One type-K thermocouple was integrated into the center coil windings, and another was bolted to the back plate to monitor the temperature of the thruster. Radiation shielding was added to the inside and outside of the discharge channel to decrease heat transfer from the channel and anode to the screens and center coil. Despite our efforts to balance the inner and outer coil currents, the optimized magnetic field required slightly more current on the outer coil to minimize the discharge current at a given operating condition. To maintain a steady-state

temperature, while the coils were operated in series together, the overall power was reduced from 1.5 kW to 1 kW to decrease the effects from the slightly imbalanced magnetic field.

A sketch of the electrical circuit used to test the laboratory model thruster is shown in Figure *2*. The electrical circuit was modified to include an RLC circuit and a variable high-power resistor that was placed in parallel with the coils, which shunted some of the discharge current and allowed fine-tuning of the magnetic field during operation. This variable resistor along with the capacitor also served to short the coil inductance at startup, mitigating the relatively large back EMF observed with the PPS 1350. Additionally, the capacitor placed across the magnet coils helped to further filter the current through the coils at startup and reduced ripple during steady-state operation. These modifications enhanced the operational stability of the thruster in addition to reducing the back EMF from the coils. In the laboratory model thruster testing, the keeper was spurred from the positive anode line on the power supply side of the RLC filter, and the resistance was reduced to $2.5\ k\Omega$. This would allow the power supply to provide sufficient current to the keeper on start up, and result in a smoother and more reliable start as noted in the work done by Ham [1].

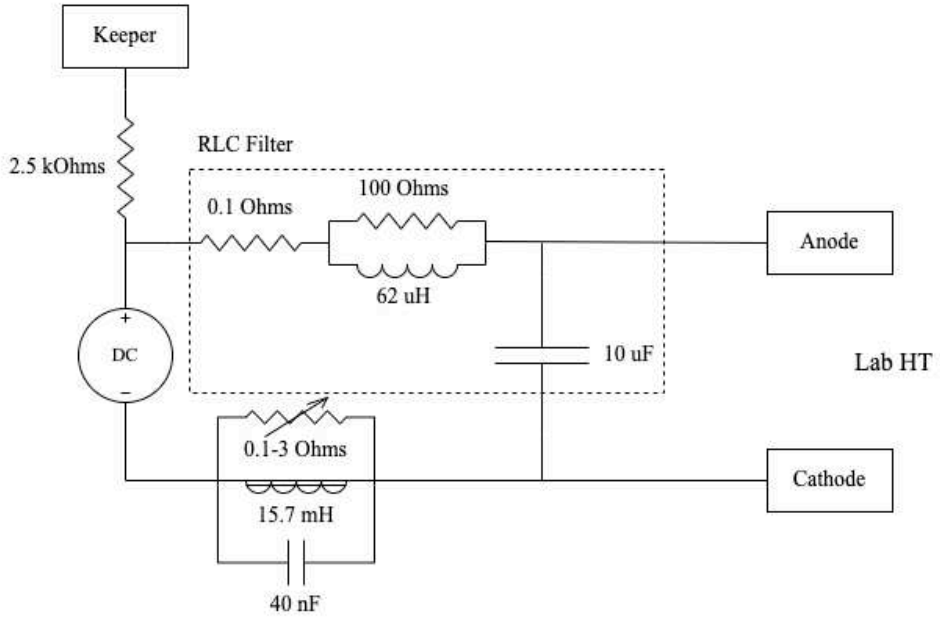

Figure 2: Modified single power supply electrical circuit used to power laboratory Hall thruster discharge.

CHAPTER 3: METHODS

The methods described here were performed to increase confidence in the measurements taken during this study by reducing systematic error. Extra care is taken to explain the way in which the thrust stand data was obtained in accordance with the recommended best practices.

Thrust Stand

A double hanging pendulum thrust stand was used to make thrust measurements. This thrust stand used a linear variable differential transformer (LVDT) to measure displacement. The LVDT has a sensitivity of 228 mV/V/mm and a linearity of 0.11% over a 20 V (0.1") range. An eddy current damper was used to damp high frequency oscillations. The double pendulum was formed by hanging a plate where the thruster is mounted by four, thin metal ribbons. Gas flow lines and electrical hookup wires that connect to the thruster, were routed to the bottom plate through waterfall and snake shaped paths to reduce the spring constant they impose on the system. This was done to help ensure that the main restorative force of the thrust stand was the gravitational force imposed when the stand was displaced.

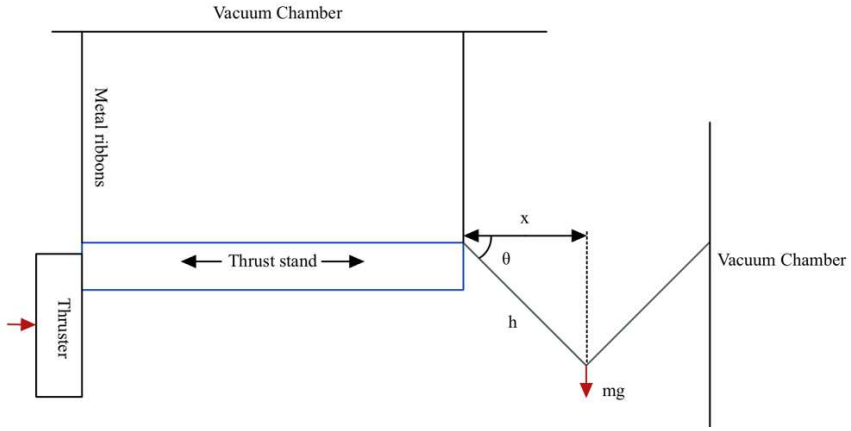

Figure 3: Calibration weight application method

Calibration was done by applying forces from hanging weights. A line was strung from the bottom plate of the pendulum to the vacuum chamber wall. The weights were hung from the center of the line applying a known axial force to the thrust stand based on the weights applied and the geometry of the line as shown in Figure *3*. There is uncertainty in the geometry of the test fixture and for small displacements this uncertainty propagates as a linear function of calibration force. The calibration force applied to the thrust stand can be described by equation 1.

$$F_{cal} = \frac{mg}{2} cot(\theta), \tag{1}$$

$$\theta = cos^{-1}(\frac{x}{h}) \tag{2}$$

In equation 1, F_{cal} is the force applied to the thrust stand by the calibration weights with mass, m, multiplied by the gravitational constant, g, and the cotangent of the angle of depression of the attached string as shown in Figure 3. The uncertainty of each measured variable in the equation is reported in Table *1*. A linear regression can be done using the data in Table 1 to predict the level of uncertainty in the LVDT output given an applied force.

Table 1: Measured variables contributing to the uncertainty of calibration force.

Variable	Measured Value	Uncertainty (+/-)
x	*0.16579 m*	*3.97E-4 m*
h	*0.254 m*	*1.27E-3 m*
m_1	*7.12 g*	*0.01 g*
m_2	*14.48 g*	*0.01 g*
m_3	*21.89 g*	*0.01 g*

A root sum of squares uncertainty analysis was also done on the known sources of error in the calibration process. This was combined with the uncertainty analysis due to random error as recommended by Polk [4]. The uncertainty in the geometry of the calibration system depends on

the length of the string and the horizontal position of the thrust stand. The masses used during the calibration process were also attributed some uncertainty. The values of each source of error in the calibration sequence provided in Table *1* were used in the root sum of squares analysis as defined in equation 3, where the function being differentiated is from equation 1.

$$e_{cal} = \sqrt{(e_x \frac{\partial F_{cal}}{\partial x})^2 + (e_h \frac{\partial F_{cal}}{\partial h})^2 + (e_m \frac{\partial F_{cal}}{\partial m})^2} \quad (3)$$

The uncertainty of a force given some measured displacement is contingent upon the uncertainty of the calibration sequence, and as shown, the uncertainty increases with force.

There are three calibration masses that are applied as previously discussed. A linearity test was done to show the response of the LVDT given a null position and the three calibration points. A continuous time series of the LVDT response is shown in Figure *4*. During this test mass was added and then removed to allow the LVDT to return to its nominal position. Each calibration point was continuously measured for 60-sec. A linear regression was fit to the averages of the LVDT response for each calibration point including the null-condition.

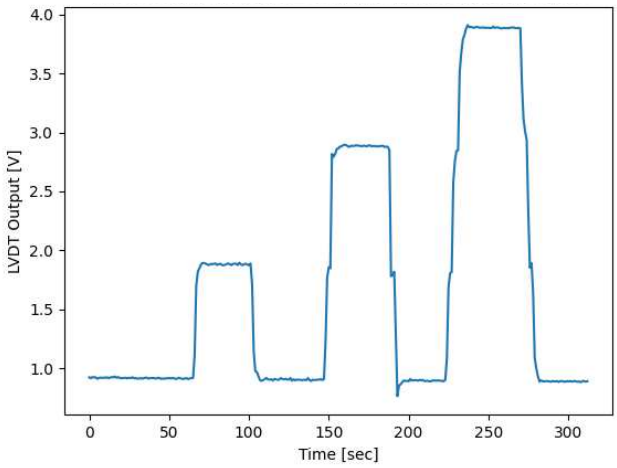

Figure 4: Thrust stand response to the application of a known force.

The typical coefficient of determination of the linear regression is $R^2 = 0.9999$. This process also determined the sensitivity of the LVDT response and is reported for each

measurement as the slope of the linear regression in millivolts per millinewton. The result of the thrust stand calibration sequence is the best fit line and the standardized residuals as shown in Figure *5*. The standardized residuals were often found to be between positive and negative two suggesting that the noise in the system is due to random sources of error rather than systematic sources.

The thrust was measured by first allowing the thruster to operate until it reached steady state (about 1-2 hr). Next the LVDT output was calculated as the average reading a period typically between 30-60 seconds. Then the thruster was turned off and the average LVDT output was recorded over a similar period. Finally, the calibration procedure was repeated, and the results of the calibration were used to determine the thrust from the difference between the LVDT readings made before and after the thruster was switched off. The calibration sequence takes roughly six minutes. It is typically observed that the null position of the LVDT begins to drift during this time due to cooling. The zero is determined from the intercept of the linear regression performed on the null position readings throughout the calibration sequence. Once the thermal drift is corrected, the slope of the regression fit to the measured calibration points is used to determine the thrust.

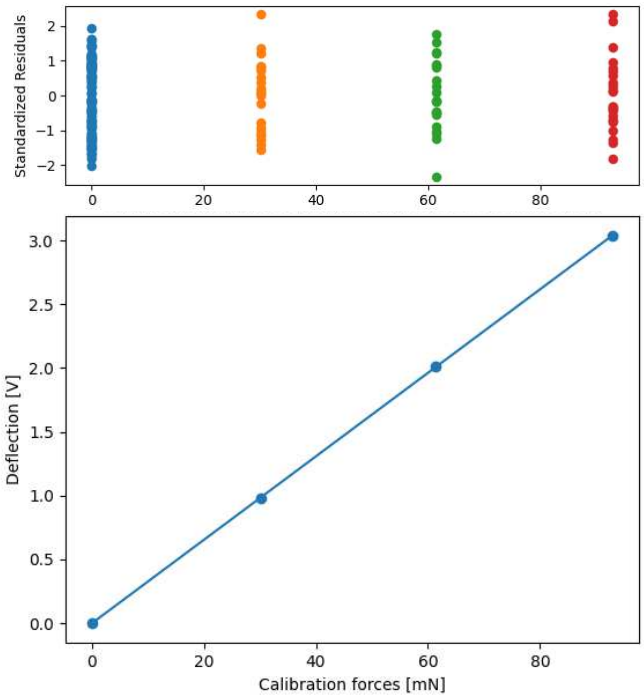

Figure 5: Thrust stand data relating deflection from known forces. The slope of the line is the sensitivity (bottom). The standard residuals are shown above and mostly remain between +/- 2 standard deviations of the mean.

Far Field Measurements

Beam ion current density profiles were measured with a magnetically shielded Faraday probe with a guard ring [5]. The probe was mounted to an arm, which was swept over an arc whose pivot point is on the thruster center line at the thruster exit plane. The arc of the arm motion was approximately 75 cm in radius with the Faraday probe facing the thruster. The collector electrode area of the Faraday probe was 1 cm^2. The collector and the guard ring were held at -20 V with respect to ground, and the collector current was determined by measuring the voltage across a 1,081 Ω resistor. The electrical circuit schematic is shown in *Figure 6*.

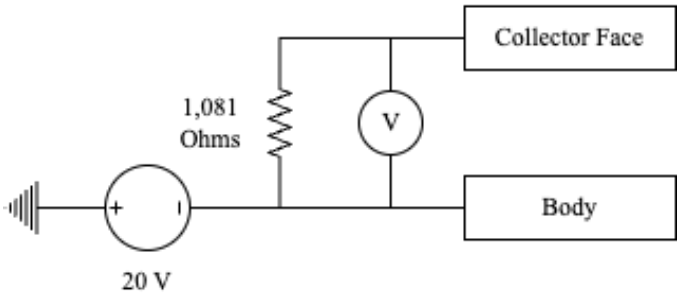

Figure 6: Faraday probe collection circuit

A retarding potential analyzer (RPA) was used to determine the ion energy distribution. The RPA was placed about 1 m from the thruster on the thruster centerline during measurement. An RPA uses a series of grids held at various potentials to discriminate between beam ions of varying energy, beam plasma electrons, and secondary electrons emitted from the probe collection face. The first grid the plasma encounters is isolated and floats at a potential about 10 volts negative of plasma potential. The second grid is held at a negative potential of 20-25 V below ground to repel beam plasma electrons. The third grid is the retarding grid that only allows ions with energy greater than the potential of this grid to pass. The fourth grid is held at 20-25 V below ground to ensure any electrons that are emitted from the collector due to ion induced secondary electron emission are returned to the collector. The collector is held at ground while the retarding grid is swept from ground potential to a potential of about 150 V greater than the beam voltage. At low biases the discriminator allows all the beam ions to pass through the grids and be collected. As the retarding potential of the discriminator rises less beam ions can pass the electric potential barrier. Eventually the collector current goes to zero when the retarding potential applied to the discriminator is greater than the highest energy beam ions. Figure *7* shows the screens and electrodes used with the RPA along with the repelled and passed charge particles.

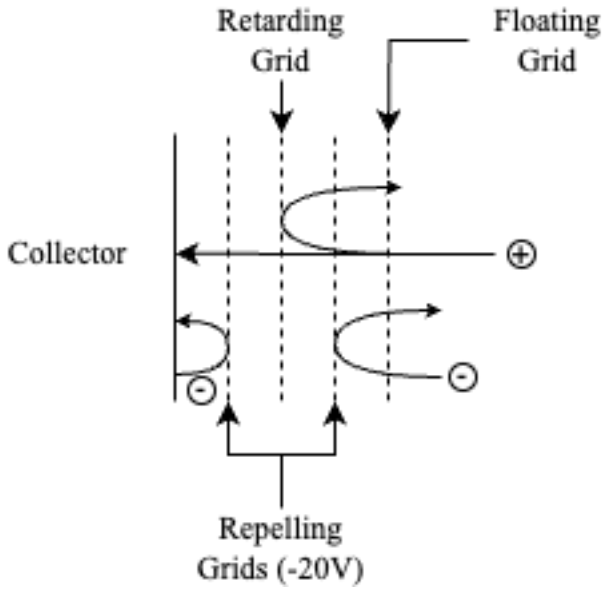

Figure 7: Retarding potential analyzer grids with depiction of repelled electrons, repelled ions, and transmitted ions.

Electrical Configurations

The thruster was tested in four distinct electrical configurations to isolate the effects of each modification and determine their impact on performance. Initially, the thruster was operated using three power supplies: one dedicated to the anode, one to the keeper, and one to the coils. This configuration served as a baseline for comparison. In the second configuration, two power supplies were used; one powered the keeper while the anode was supplied by the second power source, with the coils connected in series on the negative side of the anode power supply and upstream of the filter. This setup allowed for assessment of the thruster performance when the coils were connected in series with each other and with the anode power supply. The third configuration also utilized two power supplies but differed by powering the coils separately and connecting the keeper to the anode power supply, thereby determining if the anode voltage at startup was sufficient to start the cathode. Finally, in the fourth configuration, the thruster components were consolidated in a manner where a single power supply could be used. Figure *2*

shows this configuration. Here, the keeper was connected to the anode electrode through a 2.5 $k\Omega$ resistor, while the coils were placed in series on the negative side of the power supply (upstream of the filter). This final setup aimed to evaluate the feasibility and performance of operating the thruster with a single power supply. The same CisLunar prototype flight PPU used during the PPS 1350 testing was used here to demonstrate its capability. All four electrical configurations are compiled in *Figure -12*.

Finally, to demonstrate the reduction in back-emf on startup, an oscilloscope recorded the coil voltage and coil current in the single power supply configuration during ignition. The measurement points are shown in *Figure 8* where the ammeter, A, and voltmeter, V, are indicated.

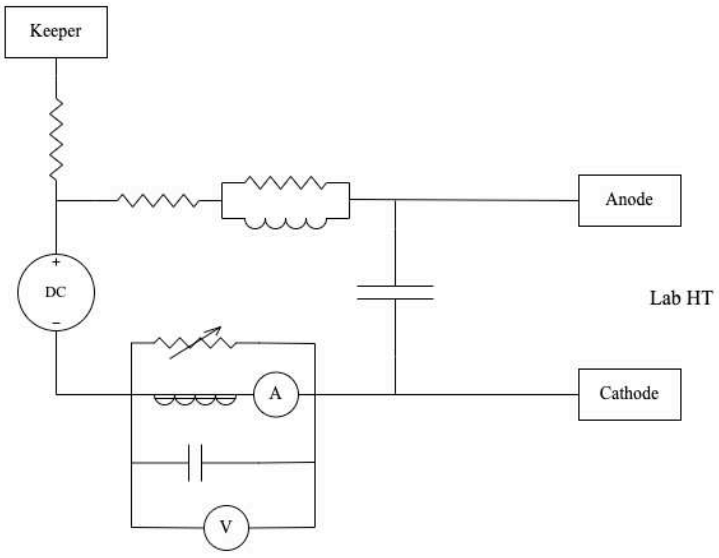

Figure 8: Oscilloscope measurement points on single power supply electrical configuration

Data collection occurred after the thruster was operated until temperature measured by thermocouples placed in the center coil and on the backplate of the thruster reached a steady state. After reaching steady state, the Faraday probe was swept in front of the thruster and an RPA trace was taken before turning the thruster off and performing a thrust measurement. Post

processing of data logs during this process provided the raw data, which were corrected in the ways described in the proceeding chapter.

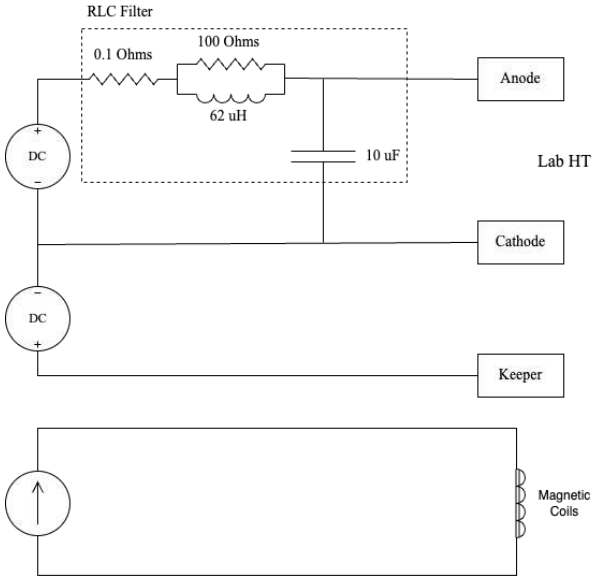

Figure 10: Multiple Power Supplies

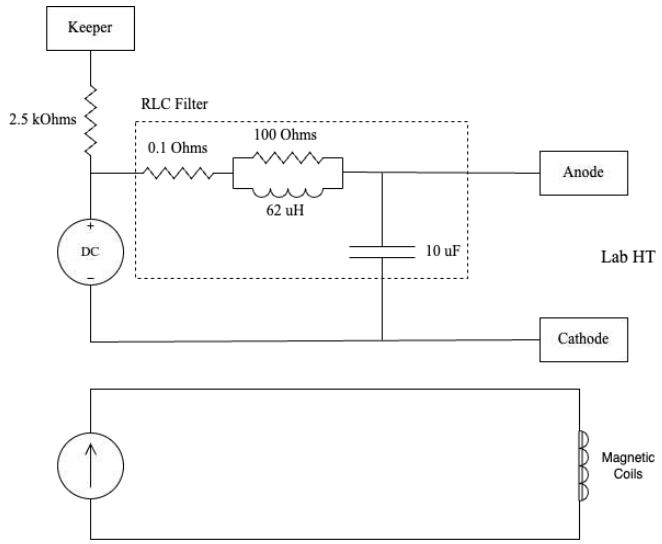

Figure 11: Spurred Keeper

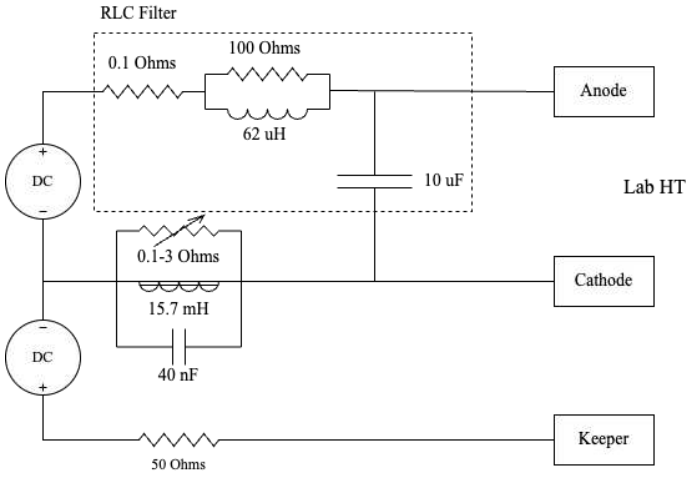

Figure 9: Coils in Series

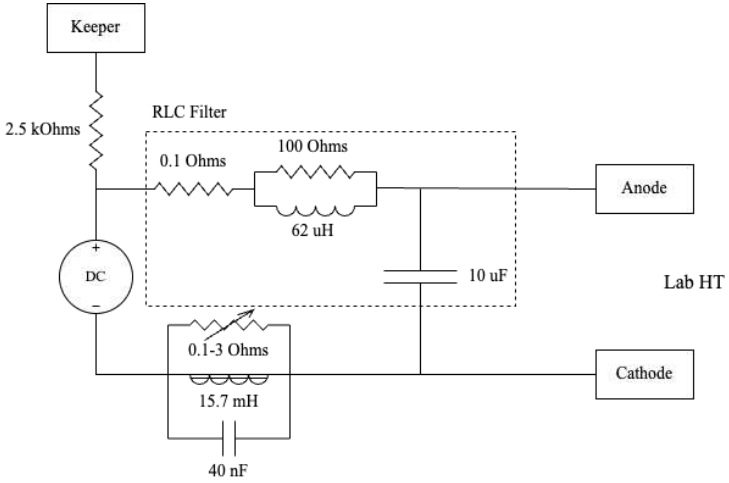

Figure 10: Single Power Supply

CHAPTER 4: ANALYSIS

The following subsections describe how the data were analyzed to obtain thruster performance parameters. After obtaining the partial pressure of krypton, a simple ingestion model was used to correct the total flow of neutrals into the ionization region. A gauge correction factor was also applied to the injected flow to the anode. Corrections were then applied to the far-field plume data because of the effect of charge exchange collisions. Finally, this chapter is summarized with a description of the anode efficiency obtained from the thrust stand as well as the phenomenological analysis performed with the data collected from a Faraday probe and retarding potential analyzer.

Pressure and Flow

Pressure and flow corrections were applied to inform charge exchange corrections, the ingestion rate, and the injected flow of krypton to the anode. The pressure was corrected using the gauge correction factor, $\beta = 1.94$, to obtain the partial pressure of krypton using equation 4.

$$P_{corr} = P_{bl} + \frac{P_{meas} - P_{bl}}{\beta} \tag{4}$$

The baseline pressure, denoted P_{bl}, was measured before testing without any flow into the chamber so that the assumption that N_2 is the primary species could be made. However, the pressure measured during testing the sum of the partial pressure of N_2 and the partial pressure of the injected gas Kr. The gauge correction factor is applied to the difference of the measured pressure, P_{meas}, and the baseline pressure, or in other words to the partial pressure of krypton. Summing the partial pressure of N_2 and Kr provide the total corrected pressure in the chamber.] during operation.

The partial pressure of Krypton was used to estimate the neutral ingestion from the vacuum chamber to the thruster. The ingestion is modeled as a function of the thermal velocity of background neutrals and the cross-sectional area of the discharge channel [6]. The injected flow into the discharge channel was controlled using an Alicat flow controller set to control krypton in sccm, thus the only correction needed is the conversion to kilograms per second. The sum of the injected flow and the ingested flow is then the total flow into the discharge channel and denoted as $\dot{m}_a$.

$$\dot{m}_a = \dot{m}_{injected} + \dot{m}_{ingested} \tag{5}$$

$$\dot{m}_{ingested} = \frac{1}{4} A n_o M \bar{c} \tag{6}$$

Where A is the front area of the discharge channel, the background neutral density is denoted n_o, the molar mass is M, and the background thermal velocity is conveyed as $\bar{c}$. The temperature of the background neutrals is assumed to be the temperature of the vacuum chamber wall which is approximately 310 kelvins and along with the measured background partial pressure of krypton provided the input to find the neutral density using the ideal gas law [7].

Retarding Potential Analyzer

After taking the negative derivative of the collected current with respect to voltage, a smoothing algorithm was used to filter the raw data and reduce the noise in the output. The algorithm used was a cubic spline approximation which was developed to avoid the Runge phenomenon when taking high order polynomial approximations. After applying the smoothing algorithm to the collected current, the central difference method was used to numerically differentiate the collected current with respect to the collector voltage. This method provides

further smoothing to the output function, which is accepted as the ion energy distribution function. The raw data and corrections are shown in Figure *12*.

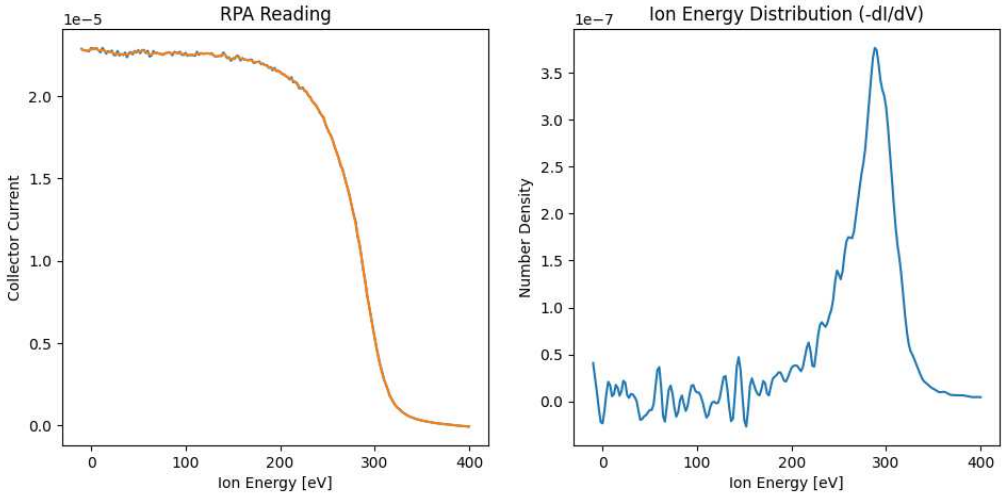

Figure 12: Raw (blue) and smoothed (orange) collector current versus collector voltage (left). Ion energy distribution function (right). Data from laboratory hall thruster running on single power supply.

The weighted average of the ion energy distribution function is taken to be the average beam energy in units eV or volts equivalent. The beam energy is used calculate the charge exchange cross collisional cross section which will be used in the analysis of the faraday probe data. It can also be used to solve for the average velocity with which the ions are exiting the thruster and is crucial in the formulation of the phenomenological efficiencies.

Faraday Probe

Charge exchange was accounted for using the findings of Hause [8] and are reiterated here in Table *2* and applied in equation 7. Where the constants *A* and *B* are the experimental results from Table *2*. The ion energy distribution was used to obtain a weighted average cross section based on the ion energy distribution function for the variable *E* in equation 7. For the purposes of this study a double to singles ratio of 0.2 was used, which is typical for a SPT-100 like Hall thruster

operated on krypton. Thus, the correction factor formulated by equation 8 is readily found given the distance x between the face of the thruster and the Faraday probe.

$$\sigma = A - B\, log_{10}(E) \tag{7}$$

$$cf = \left(1 - \frac{I^{++}}{I^{+}}\right) e^{-\sigma_1 n_0 x} + \frac{I^{++}}{I^{+}} e^{-\sigma_2 n_0 x} \tag{8}$$

Table 2: Constants found by Hause to calculate charge exchange cross section of krypton.

	A	**B**
Singles	80.7	14.7
Doubles	44.6	9.8

The correction factor from equation 8 is the proportional factor between the measured ion flux at the probe to the ion flux leaving the thruster. Thus estimating the number of ions that would be collected at the Faraday probe if no charge exchange collisions occurred. Following this correction, a second correction was applied to the wings of the ion current density profile following the approach of Huang et al [9]. Specifically, the wing regions were fit to a log-linear plot of the data between 10-20 degrees and then this fit was extrapolated from 20 out to 90 degrees. The laboratory-model Hall thruster exhibited a log-linear relationship narrower than what was recorded by Huang et al while testing the NASA-300M and NASA-300MS thrusters [9]. This is most likely due to differences in the thruster magnetic field topology. The current density profile from the laboratory Hall thruster while running on a single power supply and the log-linear plot are both shown in Figure *13*. The uncorrected raw data is shown in green, and, after extrapolating the wings out and applying the correction factor, the reconstructed current density profile is shown in blue. This technique has been accepted as a method to remove the effects of slow-moving charge exchange ions and redistribute them to the most likely trajectory before the charge exchange collision occurred.

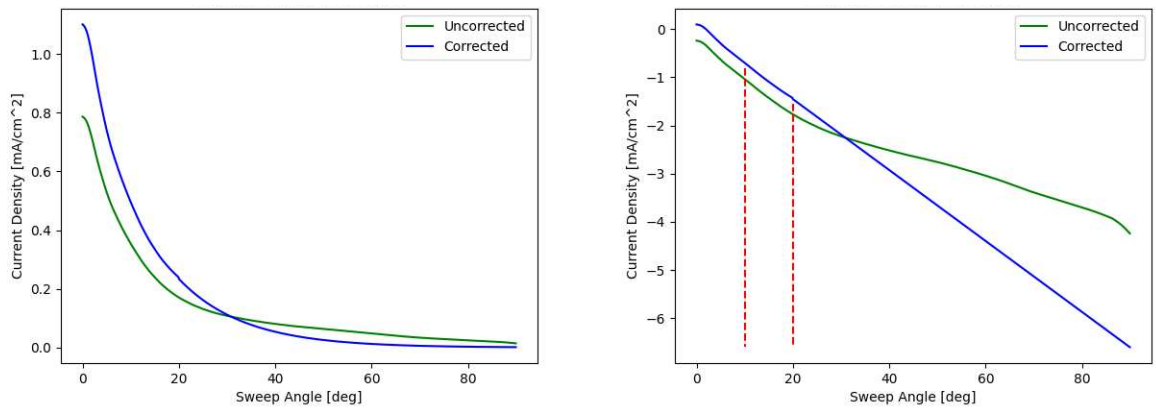

Figure 13: Linear (left) and Log (right) Current density profiles of laboratory hall thruster running on a single power supply from 0 degrees (thruster centerline) to 90 degrees. Before (green) and after (blue) correcting for charge exchange. The region of log-linear behavior is noted between the two red dashed lines.

It is of note that, if done properly, the total integrated beam current of the uncorrected (green) curve and the corrected (blue) curve should be similar, if not identical. This is due to a charge exchange collision removing a single ion from the beam and producing a slow-moving ion on the wings. Thus, the total number of ions collected should be indicative of the total number of ions leaving the thruster. In this thinking, the corrections to reconstruct the beam are most useful to determine the beam divergence which is used later to construct the phenomenological efficiencies. Other effects are proposed and discussed in the findings of Hallouin and Mazouffre [10], but their findings also support the dominance of charge exchange ions on the wings. However to be explicit on the matter, the total beam current, which will also be used later to construct the phenomenological efficiencies, was determined from the corrected (blue) curve.

It is also of note that these are relatively simple corrections. It is well-known that the facility effects on these measurements can be quite extensive or even immeasurable. More rigorous corrections are described in the recommended best practices by Brown [11], but the corrections taken here are accepted as a reasonable approximation and are implemented similarly in other studies [9].

Phenomenological Efficiencies

Phenomenological efficiencies were derived by expanding anode efficiency into plasma-diagnostic based sub-efficiencies including mass (η_m), voltage (η_v), divergence (η_d), and current (η_c) efficiencies, and a thrust correction factor (γ) for beam divergence and charge utilization. This is the form presented by Goebel and Katz [6], and it establishes an equivalence in equation 9 between phenomenological (on the left) and measured (on the right) anode efficiency. The agreement between the direct and derived methods validates thruster performance. Additionally, the phenomenological sub-efficiencies highlight underperforming areas in the thruster. This analysis method was used herein to assess the impact of various electrical configurations on thruster performance.

$$\gamma\eta_d\eta_c\eta_v\eta_m = \frac{F^2}{2\dot{m}_a P} \tag{9}$$

The thrust correction factor is applied due to the leftover charge utilization (α_m) and divergence factor from the squared thrust value. It is found through equation 10, and to reiterate the doubles to singles ratio was assumed to be 0.2.

$$\gamma = \alpha_m \cos(\theta_{div}), \alpha_m = \frac{1 + \frac{1}{\sqrt{2}}\frac{I^{++}}{I^{+}}}{1 + \frac{I^{++}}{I^{+}}} \tag{10}$$

The divergence efficiency is a single factor of the cosine of the divergence half angle, as shown in equation 11. The half angle is determined from the current density profile and is found as the angle in which the integrated current reaches 95% of the total beam current, as recommended by Brown [11].

$$\eta_d = \cos(\theta_{div}) \tag{11}$$

The current utilization is the ratio of the total beam current found with the faraday probe and the discharge current measured by the power supply. Similarly, the voltage utilization is the weighted average beam voltage (energy) determined by the ion energy distribution function and the discharge voltage measured between the anode and the cathode on the thruster side of the discharge filter. These relationships are indicated by equation 12 and 13.

$$\eta_c = \frac{I_b}{I_d} \tag{12}$$

$$\eta_v = \frac{V_b}{V_d} \tag{13}$$

Finally, the mass utilization is determined by the ratio of the total beam current and the effective current of neutral particles incident on the ionization region. In equation 14, the mass flow is depicted in kilograms per second and the molar mass (M), charge utilization (α_m), and elementary charge (q) make up the resultant unit conversion to amperes equivalent.

$$\eta_m = \frac{I_b M \alpha_m}{\dot{m}_a q} \tag{14}$$

While taking thrust measurements, a time series of the LVDT output is analyzed to produce the steady state deflection due to thrust and determine the sensitivity from the calibration process immediately after the thruster is shut off. A typical time series of the LVDT output is shown in Figure *14* alongside the resultant linear regression done on the calibration sequence. The sensitivity of the calibration measurement done after each thrust measurement produced a normal distribution around 32.87 mV/mN with a standard deviation of only 0.163 mV/mN. This indicates that the thrust stand and LVDT response were repeatable and most likely that no systematic error was present during measurements.

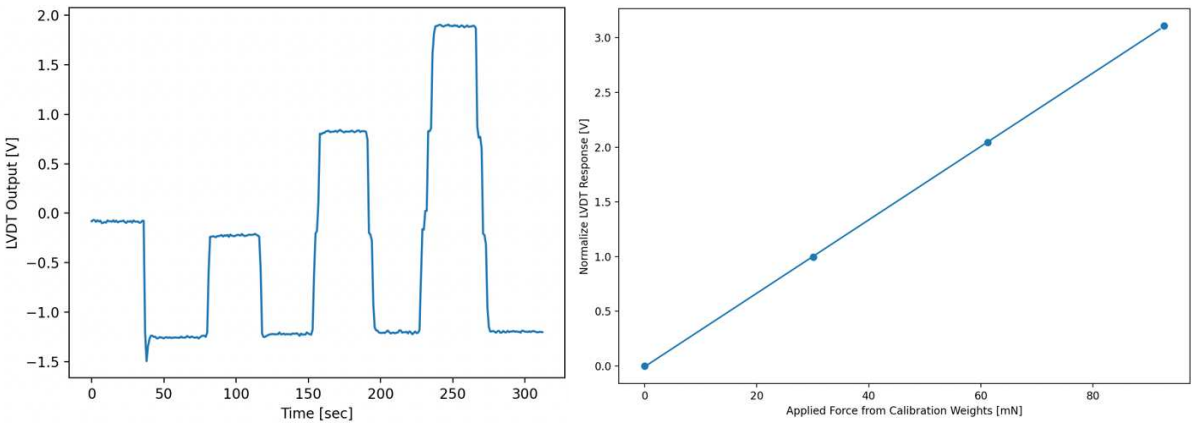

Figure 14: LVDT time series for thrust measurement of laboratory-model Hall thruster (left) and regression analysis of linear displacement from the application of known calibration weights (right).

To conclude, the first and foremost data source in this study is the anode efficiency calculated from thrust stand data. Following the procedure recommended in ref. [4], the thrust stand is quantified and presented here as a dependable source in which to draw conclusions about the performance of the thruster. Additionally, far-field plume measurements were taken, and the corrections described were applied to produce a set of phenomenological sub-efficiencies that equate to the measured thrust stand data. Finally, electrical probes were placed to observe transient effects of the electrical configuration required to operate a Hall thruster with a single power supply. These findings of these efforts are presented presently to determine the effects of running a Hall thruster on a single power supply.

CHAPTER 5: RESULTS AND DISCUSSION

The results indicate no significant difference in thruster performance with varying power supply. The modifications to the thruster were successful in providing a stable and repeatable operational state to compare the various electrical configurations. The addition of an RLC circuit to the magnet coils was proven to be a successful mitigation technique to reduce large voltages from the coils on startup that could potentially damage the coil insulation. The variable resistor tied across the magnet coils was also proven to be an effective technique to optimize the current through the magnetic coils. During start up the variable resistor was set to its nominal steady state position (~2 Ω) and the RLC component produced no more than 150 V as shown in *Figure 15*. Additionally, it is worth noting that the current in the coils does not reach its steady state value of 1.4 amps until a significant amount of time after ignition.

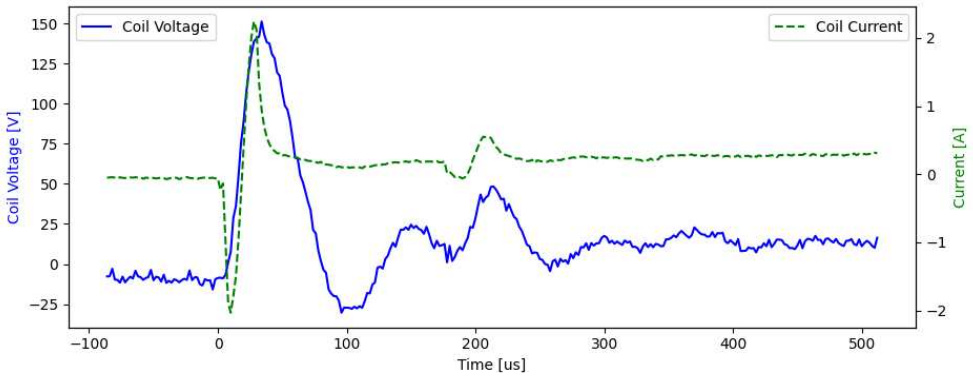

Figure 15: Coil transience during ignition of the laboratory Hall thruster in the single power supply configuration

Thrust measurements were taken in each electrical configuration detailed previously in CHAPTER 3: METHODS. The work on the thrust stand enabled accurate and repeatable results, and *Table 3* details the measured thrust, anode flow, discharge power, and the computed efficiency for each configuration.

Table 3: Measured anode efficiencies with thrust stand

	Flow [mg/s]	Voltage	Current	Thrust [mN]	Anode Efficiency
Separate Supplies	2.888	303.50	3.344	34.79 +/- 0.45	20.65%
Spurred Keeper	2.818	303.45	3.216	33.11 +/- 0.44	19.92%
Coils in Series	2.851	299.83	3.311	34.07 +/- 0.44	20.52%
Single Supply	2.897	303.52	3.228	34.29 +/- 0.45	20.19%

Analysis of the far field probe data was successful in reconstructing anode efficiency, providing a reliable assessment of the sub-efficiencies involved which are tabulated in *Table 4*. Assuming the results belong to the same population, the resultant anode efficiencies from the phenomenological analysis had a standard deviation of 0.8%. As expected, the far-field measurements produced more variant efficiencies than the thrust stand data, which had a standard deviation of 0.33%. Furthermore, two standard deviations are enough to encompass the entirety of both recorded populations. This indicates that their variation is due to random sources of error and that these data provide accurate representations of the sub-efficiencies. It is evident that at low power levels, both mass and current utilizations are most impacted. These utilizations also account for most of the variance observed in the reported phenomenological anode efficiencies. This variance can be attributed to the variability in the Faraday probe data and its analysis, which is influenced heavily by background pressure due to the corrections needed to account for charge exchange collisions.

Table 4: Measured anode efficiencies with far-field plume data

	γ	Divergence Efficiency	Mass Utilization	Voltage Utilization	Current Utilization	Anode Efficiency
Separate Supplies	0.824	0.863	0.565	0.894	0.591	21.23%
Spurred Keeper	0.824	0.863	0.548	0.892	0.581	20.20%
Coils in Series	0.828	0.867	0.538	0.901	0.561	19.52%
Single Supply	0.83	0.87	0.530	0.899	0.559	19.23%

The implications of these findings will guide further testing on the subject. The viability of the single power supply electrical configuration, coupled with an instant start hollow cathode, demonstrates the potential to reduce both complexity and the mass of the power supply. However, additional work is necessary to determine full efficiencies across a range of discharge powers. Further exploration of the electrical configuration is also warranted. Implementing a switch to stand off the discharge voltage to the keeper will reduce total power output. Additionally, splitting the RLC component into two parts could allow for fine-tuned control over the inner and outer coil currents. Further work sizing the capacitor will benefit the power dissipated across this component. A more rigorous analysis to determine the species-specific ion energy distribution would help address the assumptions made in the phenomenological analysis, particularly regarding the charge utilization. Finally, there is concern surrounding the use of instant start hollow cathodes due to the large burst of gas required for ignition. A systems level analysis could be done to determine the efficiency losses due to this. It is suggested here to include the amount of gas required for cathode ignition to obtain an equivalent flow over the entire duration of each thruster firing.

CHAPTER 6: CONCLUSION

This study has demonstrated the effectiveness of using far field probe data to reconstruct the anode efficiency in a laboratory-model Hall thruster. The findings show that there is no significant difference in anode efficiency when operating the laboratory Hall thruster with a single power supply at a discharge power of one kW compared to using multiple power supplies to operate at the same power. This result supports the viability of the single power supply configuration, which can reduce system complexity and power supply mass.

The results also highlighted that mass and current utilizations were the most impacted at the low power level and contribute significantly to the variance in anode efficiencies due to variability in Faraday probe data and the effects of background pressure. These insights will inform future testing and modifications aimed at enhancing the commercial viability of Hall thrusters powered by a single power supply.

It Is suggested the future research focus on increasing the confidence in these findings by exploring full efficiencies across a range of discharge powers while optimizing the electrical configuration. The determination of species-specific ion energy distribution will help to better inform the phenomenological analysis.

The present study's findings are valuable to the design and operational strategies of Hall thrusters for space applications. By addressing the challenges and limitations encountered, future studies can build on these findings to achieve greater efficiencies and influence systems level approaches to reduce power system cost, mass, and complexity.

REFERENCES

[1] R. Ham, J. Williams, S. J. Thompson and S. Farnell, "A low erosion instant start ignition process for Heaterless Hollow cathodes," *AIAA Propulsion and Energy 2021 Forum,* Jul 2021.

[2] R. A. Martinez, C. C. Farnell and J. A. Moritz, "Hall current plasma source having a center-mounted cathode or a surface-mounted cathode". United States of America Patent 10,269,526, 6 March 2018.

[3] C. Koppel, F. Marchandise, D. Estublier and L. Jolicet, "The SMART-1 Electric Propulsion Subsystem In-Flight Experience," in *AIAA-2004-3455, 40th AIAA/ASNE/SAE/ASEE Joint Propulsiong Conference & Ecfibit*, Fort Lauderdale, FL, 2004.

[4] J. E. e. a. Polk, "Recomended practice for thrust measurement in electric propulsion testing," *Journal of Propulsion and Power,* vol. 33, no. 3, pp. 539-555, May 2017.

[5] J. L. Rovey, M. L. R. Walker, A. D. Gallimore and P. Y. Peterson, "Magnetically Filtered Faraday Probe for Measuring the Ion Current Magnetically Filtered Faraday Probe for Measuring the Ion Current Density Profile of a Hall Thruster. Density Profile of a Hall Thruster.," *Review of Scientific Instruments,* Jan 2006.

[6] D. Goebel and I. Katz, Fundamentals of Electric Propulsion Ion and Hall Thrusters, Hoboken, NJ: Wiley, 2008.

[7] J. W. Dankanich, M. Walker, W. M. Swiatek and J. T. Yim, "Recommended Practie for Pressure Measurement and Calculation of Effective Pumping Speed in Electric Propulsion Testing," *Journal of Propulsion and Power,* vol. 33, no. 3, 2017.

[8] M. L. Hause, B. D. Prince and R. J. Bemish, "Krypton Charge Exchange Cross sections for Hall Effect Thrust Models," *Journal of Applied Physics,* vol. 113, no. 16, p. 163301, 2013.

[9] W. Huang, R. Shastry, G. C. Soulas and H. Kamhawi, "Farfield Plume Measurment and Analysis on the NASA-300M and NASA-300MS," in *33rd International Electric Prupulsion Conference*, Fairview Park, OH, 2013.

[10] T. Hallouin and S. Mazouffre, "Far-Field Characterization of a 100-W Class Hall Thruster," *Aerospace,* 2020.

[11] D. L. Brown, M. L. R. Walker, J. Szabo, W. Huang and J. E. Foster, "Recommended Practice for Use of Faraday Probes in Electric Propulsion Testing," *Journal of Propulsion and Power,* vol. 33, no. 3, May-June 2017.